The 39th International Symposium on Lattice Field Theory
Bonn, Germany, August 8 - 13, 2022
EIGHT SPECTRA OF VERY EXCITED FLUX TUBES IN SU(3) GAUGE THEORY

PEDRO BICUDO, ALIREZA SHARIFIAN, AND NUNO CARDOSO
CEFEMA, DEPARTAMENTO DE FÍSICA, INSTITUTO SUPERIOR TÉCNICO, UNIVERSIDADE DE LISBOA,
AVENIDA ROVISCO PAIS 1, 1049-001 LISBON, PORTUGAL

ABSTRACT

We compute the spectra of flux tubes formed between a static quark antiquark pair up to a significant number of excitations and for eight symmetries of the flux tubes, up to Δ_u, using pure $SU(3)$ gauge lattice QCD in 3+1 dimensions. To accomplish this goal, we use a large set of appropriate operators, an anisotropic tadpole improved action, smearing techniques, and solve a generalized eigenvalue problem. Moreover, we compare our results with the Nambu-Goto string model to evaluate possible tensions which could be a signal for novel phenomena.

INTRODUCTION

As gluons, force carries of strong forces, have color charges, the gluonic fields are squeezed in the vacuum and form a flux tube. This is in contrast to the electromagnetic fields which spread out in the space. The dominant behavior of flux tubes are string-like. A confirmation for the string-like behavior is the Regge trajectories observed in hadron spectra. The string theories also predict a linear potential between quarks which is confining and reproduces correctly the confinement of quarks inside hadrons.
Quantization of a relativistic string leads to a tower of excitations, however different theoretical models exist for the excitations of hadrons, such as bag models for different sorts of hadrons, or a few-body potentials for mesons, baryons or hybrids. Therefore, a first principle computation is important to test these models and search for novel phenomena. Numerous lattice QCD calculations have been devoted to study the excitation of the flux tube [1, 2], however, they only succeeded to compute a small number of excitations, up to two excitations for the most amenable symmetries of the flux tube. In this work, we continue our previous study of the Σ_g^+ spectrum [3] and compute a significant number of excitations for other symmetries of the flux tube. We also compare our results with the Nambu-Goto string model.

1 Nambu-Goto model

The Nambu-Goto string model is defined by the action

$$S = -\sigma \int \mathrm{d}^2\Sigma, \tag{1}$$

where σ is the string tension and Σ is the surface of the worldsheet swept by the string. The energy of an open relativistic string with length R and fixed ends is obtained as

$$V(R) = \sqrt{\sigma^2 R^2 + 2\pi\sigma(N - (D-2)/24)}, \tag{2}$$

where N is the quantum number for string vibrations and D is the dimension of space time. This expression is known as the Arvis potential [4].

2 Symmetries of the flux tube

There are three constants of motion whose eigenvalues are used to label the quantum state of the flux tube:

- z-component of angular momentum $\Lambda = 0, 1, 2, 3, \ldots$, they are typically denoted by greek letters $\Sigma,\ \Pi,\ \Delta,\ \Phi, \ldots$, respectively
- Combination of the charge conjugation and spatial inversion with respect to the mid point of the charge axis operators $\mathcal{P}o\mathcal{C}$, its eigenvalues $\eta = 1, -1$, they are denoted by $g,\ u$, respectively.
- For $\Sigma(\Lambda = 0)$, reflection with respect to a plan containing the charge axis, $\mathcal{P}_x$, with eigenvalues $\epsilon = +, -$.

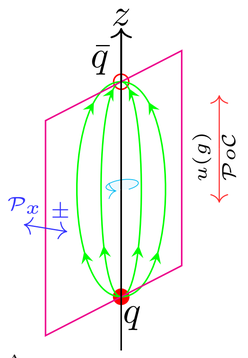

The possible quantum numbers are: $\Sigma_g^+, \Sigma_g^-, \Sigma_u^+, \Sigma_u^-, \Pi_g, \Pi_u, \Delta_u, \Delta_g, \ldots$

3 Tadpole improved action

In this work, we use the tadpole improved action on anisotropic lattices which is defined as,

$$S_{\rm II} = \beta\Big(\frac{1}{\xi}\sum_{x,s>s'}\Big[\frac{5W_{s,s'}}{3u_s^4} - \frac{W_{ss,s'} + W_{s,s's'}}{12u_s^6}\Big] + \xi\sum_{x,s}\Big[\frac{4W_{s,t}}{3u_s^2u_t^2} - \frac{W_{ss,t}}{12u_s^4u_t^2}\Big]\Big), \tag{3}$$

where $\beta = 6/g^2$ is the so-called inverse coupling and ξ is the bare anisotropic factor defined as the ratio of spatial lattice spacing to temporal lattice spacing (a_s/a_t). Furthermore, $W_c = \frac{1}{3}\sum_c \Re e\ \mathrm{Tr}(1 - U_c)$ where U_c are the closed loops shown in Fig. (1). Tadpole improvement factors $u_s = \langle\frac{1}{3}\Re e\ \mathrm{Tr}U_{s,s'}\rangle^{1/4}$ and $u_t = \langle\frac{1}{3}\Re e\ \mathrm{Tr}U_{s,t}\rangle^{1/2}/u_s$. This action has a smaller discretization error than the standard Wilson actions. Anisotropic actions ($\xi > 1$) have more time slices in plateaux compared to isotropic ones ($\xi = 1$) as well. As a result, we obtain a better estimation for the effective mass [5].

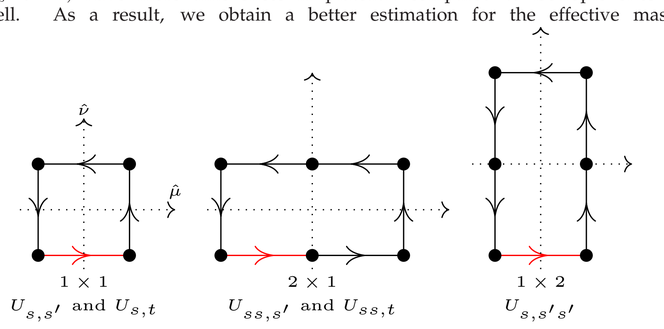

Fig. 1: Closed loops U_c are in the anisotropic tadpole improved action of Eq. (3). The redlink is updated in each step of the Monte Carlo method.

In the following table, we listed the properties of pure $SU(3)$ gauge configurations used in this work:

β	ξ	ξ_R	volume	u_s	u_t	$a_s\sqrt{\sigma}$	$a_t\sqrt{\sigma}$	Smearing (space,time)	No. of configs
4	4	3.6266(32)	24×96	0.82006	1	0.3043(3)	0.0839(1)	$Stout^{20}_{0.15}$,Multihit(100)	1060

Table 1: Properties of the pure $SU(3)$ gauge configurations generated by the action of Eq. (3). ξ_R is the renormalized anisotropic factor.

4 Obtaining the excitations

To compute the spectra of the flux tube, we first compute the Wilson correlation matrix $\mathcal{C}(r,t)$. The entry $\mathcal{C}_{i,j}(r,t)$ of the Wilson correlation matrix is the expectation value of spatial-temporal closed loops, Fig. (2), whose spatial sides are replaced with operators O_i and O_j having identical symmetry to the flux tube of interest.

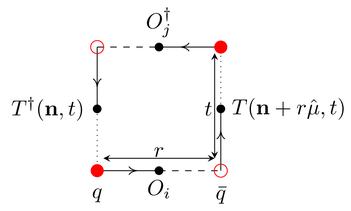

Fig. 2: A closed loop corresponds to the entry $\mathcal{C}_{i,j}(r,t)$ of the correlation Wilson matrix.

Afterwards, we find generalized eigenvalues λ of the Wilson correlation matrix,

$$\mathcal{C}(r,t)\vec{\nu}_n = \lambda_n(r,t)\mathcal{C}(r,t_0)\vec{\nu}_n, \tag{4}$$

where we set $t_0 = 0$. Consequently, we obtain a set of time dependent eigenvalues $\lambda_n(t)$ for each r. Then, we order the eigenvalues and plot the effective mass defined as

$$E_i(r) = \ln\frac{\lambda_i(r,t)}{\lambda(r,t+1)}. \tag{5}$$

The plateau in the effective mass plot corresponds to the energy $E_i(r)$.
Note that plateaux usually appear in large time values where contamination from excited states are suppressed; however, effective mass plots for large t are very noisy. To circumvent this problem, we apply stout and multihit smearing for spatial and temporal gauge links, respectively.

5 Analysis our results

When we compare our result with the Nambu-Goto spectrum Eq. (3), we observe excited states departure from the Nambu-Goto model. To quantify this tension, we fit our results to

$$V_1(R) = \sigma R\sqrt{1 + \frac{2\pi}{\sigma_2 R^2}(N - (D-2)/24)}, \tag{6}$$

where $\sigma_2 < 1$ corresponds to a larger gap between excited states than in the Nambu-Goto string model. We fit the data of all excitations with clear signals to Eq. (6). Note that the corresponding excitation number N is fixed and we exclude the data for small charge separations r. This deviation can be interpreted as the existence of constituent gluons in the more excited states.

RESULTS

6 Operators

In this part, we introduce the operators used for different symmetries of the flux tube. These operators are selected such that they lead to a smaller energy for the ground state of each symmetry and lead to smaller noises for the excited states as well. Moreover, we opt out the operators that lead to degeneracies in the spectra. The idea is to select operators with different distances l from the charge axis to sweep the width of the flux tube as much as possible. Because the spatial length of our lattice is 24 lattice spacings and it has periodic boundary conditions, we select the value of l up to 12 lattice links.

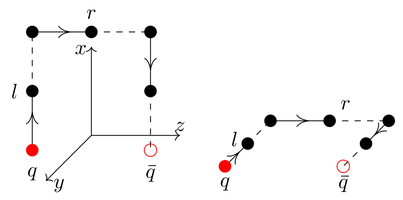

i: $O_x(l,0)$ ii: $O_y(0,-l)$

$$O^{\Sigma_g^+}(l,0) = \frac{1}{2}\big(O_x(l,0) + O_y(l,0) + O_x(-l,0) + O_y(0,-l)\big)$$
$$O^{\Pi_u^+}(l,0) = \frac{1}{2}\big(O_x(l,0) + \mathrm{i}O_y(l,0) - O_x(-l,0) - \mathrm{i}O_y(0,-l)\big)$$
$$O^{\Delta_g^+}(l,0) = \frac{1}{2}\big(O_x(l,0) - O_y(l,0) + O_x(-l,0) - O_y(0,-l)\big)$$

- Selecting l from 0 (for Σ_g^+) or 1 to 12, we construct 13 or 12 operators.

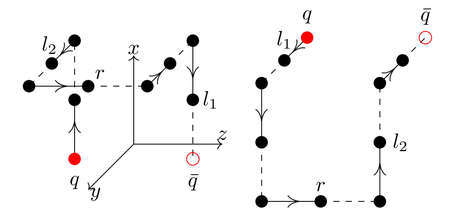

i: $O_x(l_1,l_2)$ ii: $O_y(l_1,-l_2)$

$$O^{\Sigma_g^-}(l_1,l_2) = \frac{1}{2\sqrt{2}}\Big(O_x(l_1,l_2) - O_x(l_1,-l_2) - O_x(-l_1,l_2) + O_x(-l_1,-l_2) + O_y(l_1,-l_2) - O_y(l_1,l_2) + O_y(-l_1,l_2) - O_y(-l_1,-l_2)\Big)$$

- We fix $l_1 = 1$ and let l_2 vary from 1 to 12, so we end up with 12 operators.

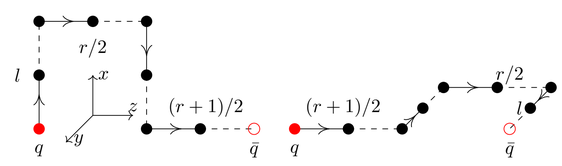

i: $O_x^L(l,0)$ ii: $O_y^R(-l,0)$

$$O^{\Sigma_u^+}_{1/2}(l,0) = \frac{1}{2\sqrt{2}}\Big(O_x^L(l,0) + O_y^L(l,0) + O_x^L(-l,0) + O_y^L(-l,0) - O_x^R(-l,0) - O_y^R(-l,0) - O_x^R(l,0) - O_y^R(l,0)\Big)$$
$$O^{\Pi_g^+}_{1/2}(l,0) = \frac{1}{2\sqrt{2}}\Big(O_x^L(l,0) + \mathrm{i}O_y^L(l,0) - O_x^L(-l,0) - \mathrm{i}O_y^L(-l,0) - \big[O_x^R(l,0) + \mathrm{i}O_y^R(l,0) - O_x^R(-l,0) - \mathrm{i}O_y^R(-l,0)\big]\Big)$$
$$O^{\Delta_u^+}_{1/2}(l,0) = \frac{1}{2\sqrt{2}}\Big(O_x^L(l,0) - O_y^L(l,0) + O_x^L(-l,0) - O_y^L(-l,0) - \big[O_x^R(l,0) - O_y^L(l,0) + O_x^R(-l,0) - O_y^R(-l,0)\big]\Big)$$

- We vary l from 1 to 12 to build up 12 operators.

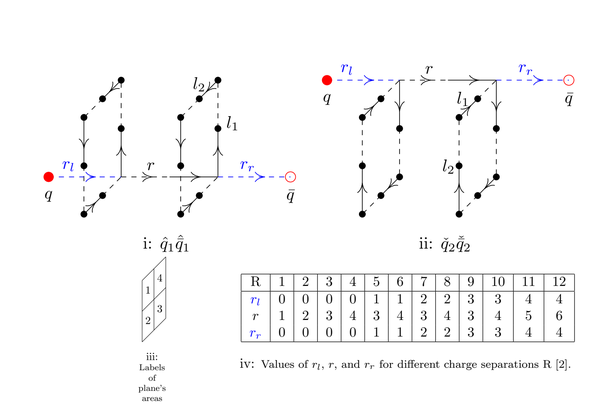

i: $\hat{q}_1\hat{\bar{q}}_1$ ii: $\hat{q}_2\hat{\bar{q}}_2$

iii: Labels of plane's areas

R	1	2	3	4	5	6	7	8	9	10	11	12
r_l	0	0	0	0	1	1	2	2	3	3	4	4
r	1	2	3	4	3	4	3	4	3	4	5	6
r_r	0	0	0	0	1	1	2	2	3	3	4	4

iv: Values of r_l, r, and r_r for different charge separations R [2].

$$O^{\Sigma_u^-}_{\square}(l,l) = \frac{1}{2\sqrt{2}}\Big(\hat{q}_1\hat{\bar{q}}_1 + \hat{q}_2\hat{\bar{q}}_2 + \hat{q}_3\hat{\bar{q}}_3 + \hat{q}_4\hat{\bar{q}}_4 - \check{q}_4\check{\bar{q}}_4 - \check{q}_3\check{\bar{q}}_3 - \check{q}_2\check{\bar{q}}_2 - \check{q}_1\check{\bar{q}}_1\Big)$$

- We select $l_1 = l_2$ and let l_1 vary from 1 to 12 to construct 12 operators.

7 Spectra of different flux tube symmetries

In the following figures, we show the obtained spectra for different symmetries of the flux tube, up to Δ_u and as a function of the charge distance R. To set the scale, we fit the ground state of Σ_g^+ to $V(r) = V_0 + \sigma r$. Then, we use σ to present our results in the string tension unit $\sqrt{\sigma}$.

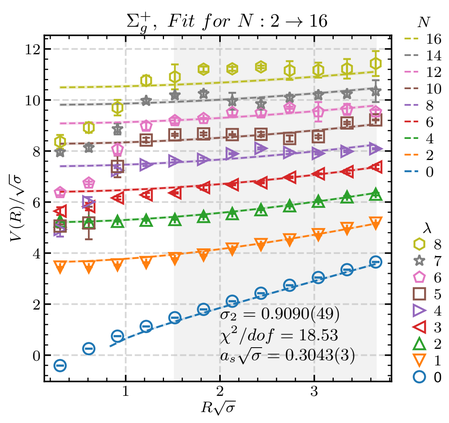

Fig. 3: Σ_g^+ spectra, the data derived from [3].

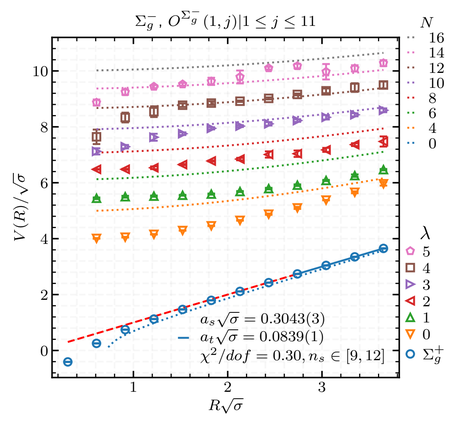

Fig. 4: Σ_g^- spectra. The solid line shows $V(r) = V_0 + \sigma r$ fitted to the ground state and dotted lines show the Arvis potential, Eq. (2).

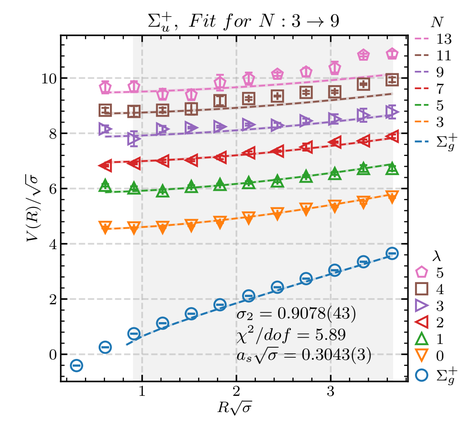

Fig. 5: Σ_u^+ spectra

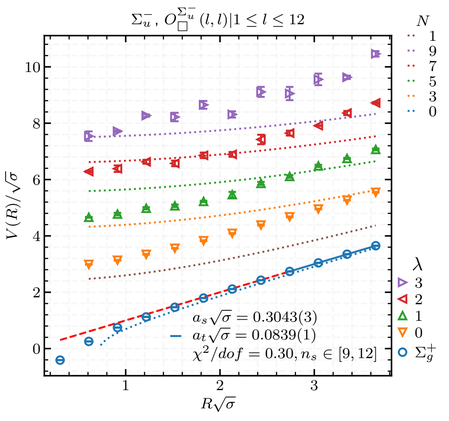

Fig. 6: Σ_u^- spectra. The solid line shows $V(r) = V_0 + \sigma r$ fitted to the ground state and dotted lines show the Arvis potential, Eq. (2).

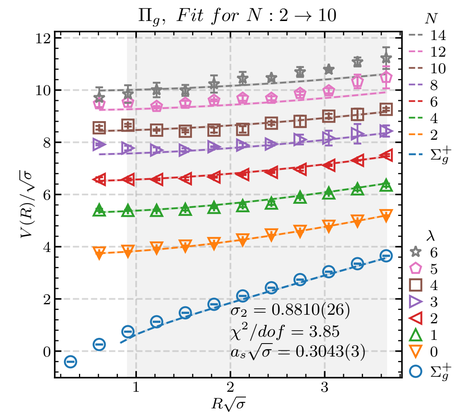

Fig. 7: Π_u spectra.

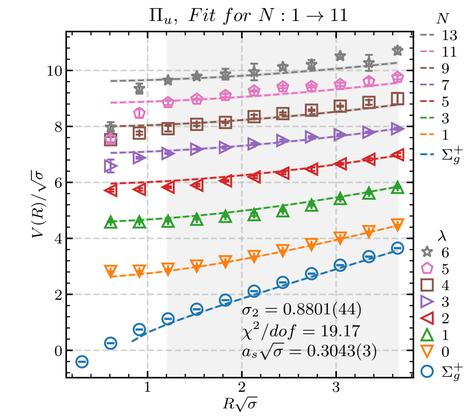

Fig. 8: Π_u spectra.

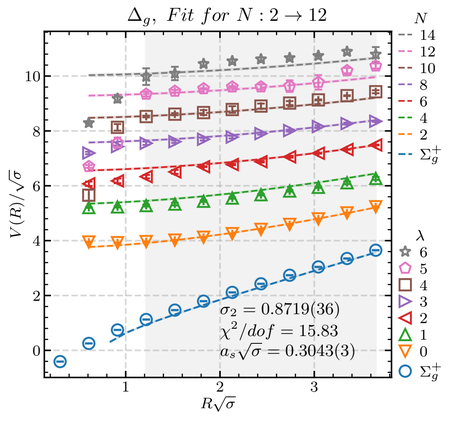

Fig. 9: Δ_g spectra.

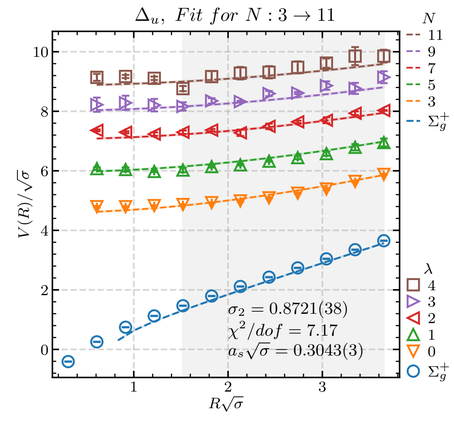

Fig. 10: Δ_u spectra.

- In the above figures, dashed lines show the spectrum of the modified Nambu-Goto ansatz Eq. (6), and dotted lines show the spectrum of the Nambu-Goto model Eq. (2).
- The width of highlighted areas around dashed lines shows the error of the fits.
- The vertical gray highlighted areas show the interval of charge separations r included in the fit.
- $\lambda = 0, 1, \ldots$ show the ground state, first excited, and so on. For each λ, the corresponding Nambu-Goto level N has the same color as the data.
- Fitted for $N_i \to N_f$ denotes the interval of N included in the multifit to Eq. (6).
- We did not fit the Σ_g^- and Σ_u^- spectra to Eq. (6) because their ground states slope is steeper than the corresponding Nambu-Goto level.

CONCLUSION

We succeeded to compute a significant number of excitations for different symmetries of the flux tube, improving the state of the art, Table. (2). Considering a second parameter σ_2 in the Arvis potential, Eq. (6), results in better fits to the data. The values of σ_2 are almost 10% smaller than σ, Fig. (11), leading to larger energy splitting between energy levels than the Nambu-Goto spectrum. This tension can be a signal for the existence of a constituent gluon in the excited flux tubes. As the χ^2/dof of the fits are large, we should take this deviation with a grain of salt.

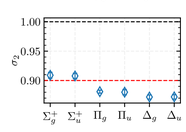

Fig. 11: Values of σ_2 for different symmetries of the flux tube.

Λ_η^+	Σ_g^+	Σ_g^-	Σ_u^+	Σ_u^-	Π_g	Π_u	Δ_g	Δ_u
S_{II}	2	0	0	0	1	1	1	0
	8	5	4	2	6	6	6	4

Table 2: The first row shows the number of excitations are already reported in the literature [1], the second row show our results.

REFERENCES

[1] K. Jimmy Juge, Julius Kuti, and Colin Morningstar. Fine structure of the QCD string spectrum. *Physical Review Letters*, 90(16), Apr 2003.

[2] Stefano Capitani, Owe Philipsen, Christian Reisinger, Carolin Riehl, and Marc Wagner. Precision computation of hybrid static potentials in SU(3) lattice gauge theory. *Phys. Rev. D*, 99:034502, Feb 2019.

[3] P. Bicudo, N. Cardoso, and A. Sharifian. Spectrum of very excited Σ_g^+ flux tubes in SU(3) gauge theory. *Phys. Rev. D*, 104(5):054512, 2021.

[4] J.F. Arvis. The exact $q\bar{q}$ potential in nambu string theory. *Physics Letters B*, 127(1):106–108, 1983.

[5] Colin Morningstar. Improved gluonic actions on anisotropic lattices. *Nuclear Physics B - Proceedings Supplements*, 53(1-3):914–916, Feb 1997.

ACKNOWLEDGMENT

Alireza Sharifian and Nuno Cardoso are supported by FCT under the Contract No. SFRH/PD/BD/135189/2017 and SFRH/BPD/109443/2015, respectively. The authors thank CeFEMA, an IST research unit whose activities are partially funded by FCT contract UIDB/04540/2020 for R&D Units.